Simulations suggest a scaffolding mechanism of membrane deformation by the caveolin 8S complex

Sayyid Yobhel Vasquez Rodriguez[1] , Themis Lazaridis*[2],

1. CCNY Undergraduate Program, Biology Sophomore

2. Department of Chemistry,
City College of New York/CUNY, 160 Convent Ave, New York, NY 10031, USA

Graduate Programs in Chemistry, Biochemistry, and Physics,
The Graduate Center, City University of New York,365 Fifth Ave., New York, NY 10016, USA

* Tel. (212) 650-8364 Email: tlazaridis@ccny.cuny.edu

Abstract

Caveolins form complexes of various sizes that deform membranes into polyhedral shapes. However, the recent structure of the 8S complex was disk-like with a flat membrane-binding surface. How can a flat complex deform membranes into nonplanar structures? Molecular dynamics simulations revealed that the 8S complex rapidly takes the form of a suction cup. Simulations on implicit membrane vesicles determined that binding is stronger when E140 gets protonated. In that case, the complex binds must more strongly to 5 and 10-nm radius vesicles. A concave membrane binding surface readily explains the membrane-deforming ability of caveolins by direct scaffolding. We propose that the 8S complex sits at the vertices of the caveolar polyhedra, rather than at the center of the polyhedral faces.

Keywords: Caveolae, molecular dynamics, lipid bilayer, membrane curvature.

Running title: Membrane deformation by caveolin

INTRODUCTION

Caveolae are invaginations in the plasma membrane of mammalian cells that have a distinct lipid composition enriched in cholesterol and glycosphingolipids (1). Their functions may include resistance to mechanical stress, mechanosensation, regulation of signaling, cholesterol homeostasis, trafficking, and endocytosis (2). Two proteins are essential for their formation: caveolins (3) and cavins (4). In humans there are three isoforms of caveolin and four isoforms of cavin. Caveolins by themselves have the capacity to deform the plasma membrane (5, 6) but formation of canonical caveolae also requires cavins.

Caveolin-1, the most prevalent isoform, has 178 residues organized in several domains: an unstructured N-terminal domain, the Oligomerization Domain (61-101) which includes the Scaffolding Domain (82-101), the so-called Intramembrane Domain (IMD) 101-134, and the C-terminal domain. Caveolin was classified as an integral membrane protein based on its strong attachment to membranes (7). This and its topology (both termini in the cytoplasm) led to the proposal that the IMD inserts as a helical hairpin and acts as a wedge to deform the membrane (8). The monomeric IMD domain in detergent adopted a helix-break-helix structure (9). On the basis of this hypothesis, several theoretical studies explored the properties of the membrane embedded hairpin (10–13).

However, a recent cryoEM structure of the 8S complex showed a picture that was more reminiscent of a peripheral membrane protein (14). The complex contained 11 protomers with the CSD, the IMD, and much of the Ct domain helical, ending in an unusual beta barrel with hydrophobic interior formed by the C-terminal ends. The paradox with this fascinating structure is that it presents a flat membrane binding surface, which was proposed to bind and stabilize flat faces of polyhedra. But then, what causes the membrane bending?

We conducted molecular dynamics simulations of the 8S in implicit solvent and found that the complex rapidly takes a conical shape with a concave membrane binding surface. An all-atom simulation in solution also showed the same shape change. Binding to membranes was especially strong with protonation of the unique charged residue E140 on the hydrophobic face. We then used an implicit solvent model for curved membranes to calculate the binding energy to vesicles of different radius and found the strongest binding to vesicles of 5 and 10 nm radius. This finding offers a clear mechanism for membrane curvature generation by caveolins.

METHODS

The simulations in solution used either the implicit solvent energy function EEF1 (15) or an all-atom representation with the TIP3P water model and the CHARMM36 force field for the protein (16). In the latter, the simulation box was rectangular with sides 186.6, 186.6, and 93.3Å. It contained 99541 water molecules and 33 K+ ions that were added to neutralize the unit cell, bringing the total number of atoms to about 317,500. The nonbonded cutoff was 12 Å and Particle Mesh Ewald was used for long range electrostatics. The simulation was run at constant temperature of 303 K using the Hoover thermostat and constant pressure of 1 atm using the Langevin piston barostat. The length of the implicit solvent simulation was 5 ns and of the all-atom simulation 3 ns.

The membrane simulations used the IMM1 model (17) and its extension to curved membranes (18), which was previously applied to ESCRT-III snf7 (19) and IBAR domains (20). Surface charge for the flat membrane was modeled using the Gouy-

Chapman theory (21). The molecular dynamics (MD) simulations were carried out with the EEF1 module of the CHARMM software package (22). The simulations were run at 300 K with a 2-fs time step for 2 ns, a time that was found sufficient for convergence of the structural change in solution. Due to the lack of solvent friction, the true time-scale of implicit solvent simulations is longer than their nominal duration.

Membrane binding energies were estimated as average transfer energies, i.e. the difference in energy of the peptides on the membrane surface and the same conformation in bulk water. This is approximate, because it neglects possible changes in intramolecular energy (including such changes makes the results very noisy). Conformational and translational entropy is also neglected in these calculations, but these contributions are likely to be very similar in binding to membranes of different curvature.

The shape of the complex was monitored by first orienting the complex parallel to the xy plane and then measuring its extent in the x, y, and z directions (largest minus smallest coordinate) as a function of simulation time.

RESULTS

Simulations in solution

We started with a 5-ns MD simulation of the 8S complex in aqueous solution using the EEF1 implicit solvation model (15). The overall structure was well-maintained but the shape rapidly changed from flat to conical (Fig. 1). Fig. 2 shows the backbone RMS deviation from the initial and final structure and the extent of the complex in the x, y, and z directions when aligned with the xy plane. There is a rapid increase in the height (Δz) of the complex from 40 to about 60 Å. The diameter does not change much, except for a transient increase in the beginning and some loss of symmetry. The changes converge in about 2 ns.

To check the validity of this approximate implicit solvent energy function the complex was also simulated in all-atom aqueous environment. This size of the system restricted us to only 3 ns but that was sufficient to show a similar structural change as the one observed in the EEF1 simulations, albeit more modest (Fig. 3). The backbone RMSD reaches about 6.5 Å (compared to 10 Å with EEF1). The width of the complex increased from 40.1 to about 56 Å (compared to 60 Å with EEF1) and the diameter decreased to about 130 Å, with more symmetry maintained than with EEF1. The smaller changes may be partly due to the slower evolution of the all-atom system due to solvent friction.

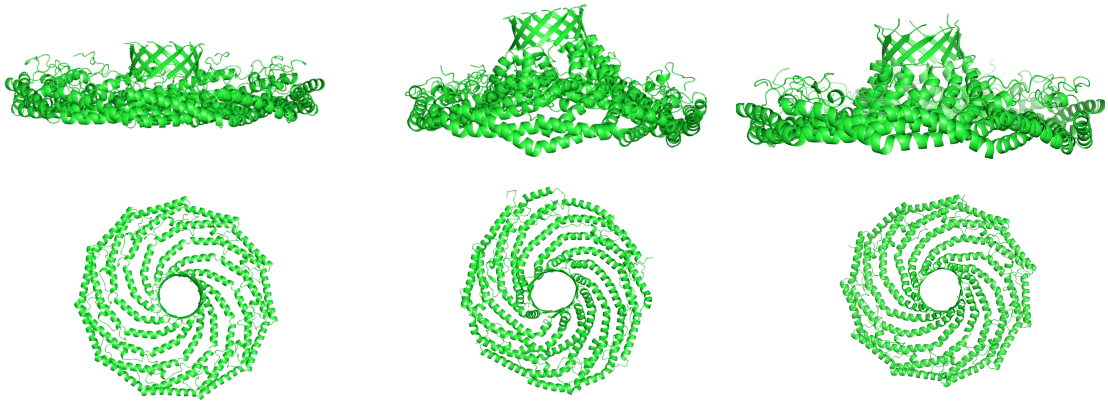

Fig. 1. Structure of 8S before simulation (left), after a 5-ns MD simulation in implicit solvent (middle), and after a 3-ns MD simulation in explicit solvent (right). Side views above and top views below.

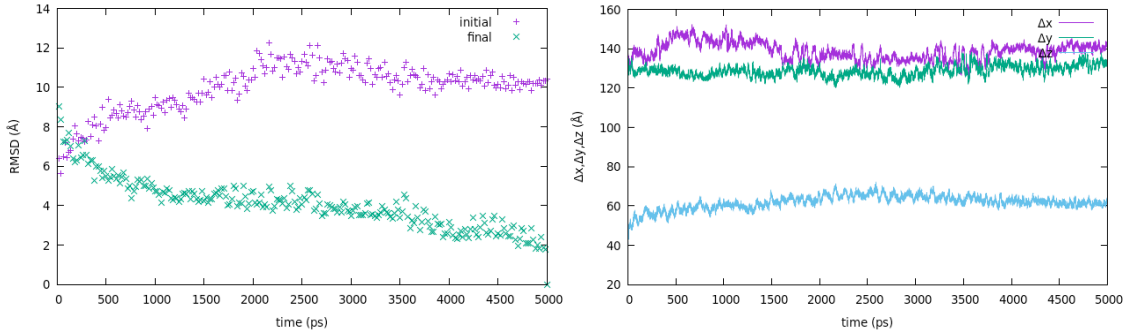

Fig. 2. 5-ns implicit solvent simulation in solution. a) Backbone RMS deviation with respect to the initial and the final structure, b) Spatial extent of the complex (the values for the cryoEM structure are 137.4, 137.4, 40.1 Å)

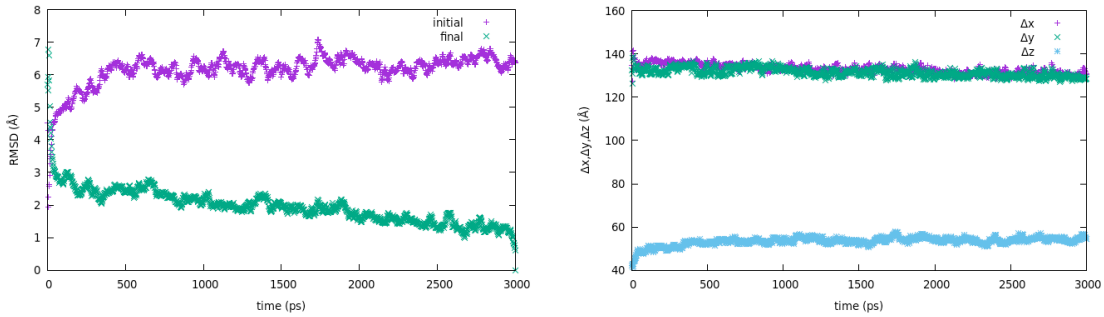

Fig. 3. Backbone RMSD (a) and spatial extent (b) and as a function of time in a 3-ns all-atom simulation in water.

The reason for the conformational change is easier to investigate in the implicit solvent runs. We did that in two ways. First, the reduction in effective energy was decomposed into contributions. It was found that both intrachain and interchain interactions improve, but the intrachain energy change is larger and comes mainly from improvement within the backbone and in the side chain-backbone interactions. Second, simulations were performed with parts of the structure constrained. It was found that constraining the backbone of residues 81-177 of each chain separately prevents the shape change. So, it is the change in backbone structure of each chain that causes the change. Among these, the largest effect on the shape change is made by residues 118-148. It seems that the simulation tries to lower the system energy by mending the various defects in the helix and this draws the middle section of the disk higher toward the C-terminal barrel, giving it a more conical shape and making the membrane binding surface more concave.

Simulations on implicit flat and curved membranes

To examine the interaction of 8S with membranes we used the IMM1 implicit membrane model (17) and its extension to curved membranes (18). The complex was placed with its flat hydrophobic face at the interface of an implicit membrane. The conformational change observed in solution also occurred on the membrane. The complex binds strongly and the outer ridge buries quite deeply in the membrane (Fig. 4),

as predicted (14). Most deeply buried is F107, which reaches 1.5 Å from the center of the membrane. However, the central region of the disk does not insert. The presence of negative surface charge on the flat membrane did not improve the binding but instead weakened it somewhat when E140 was ionized (Table 1). The basic residues in 8S are on top of the complex and far from the membrane surface, so they do not feel the surface charge.

We noticed that the only charged residue on the membrane binding face is E140, which, especially in its ionic form, is repulsed by the membrane surface. Protonation of a Glu costs only 2.3RT(pKa-pH), i.e., assuming a standard pKa and neutral pH, about 3.5 kcal/mol, or 38 kcal/mol for the entire complex. So, we also conducted simulations with E140 protonated.

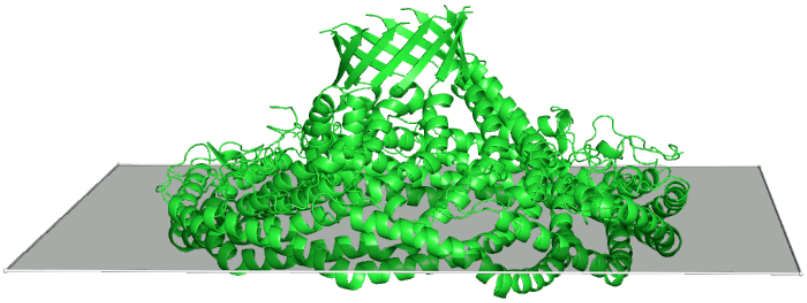

Fig. 4. Conformation of 8S on a flat, neutral implicit membrane.

Table 1. Average transfer energies (kcal/mol) of caveolin 8S from water to the membrane surface. The middle column is for ionized E140 and the right column for protonated E140.

Radius (nm)	ΔW ($E140^-$)	ΔW (E140-H)
5	-92 ± 15	-332 ± 37
10	-224 ± 43	-313 ± 50
25	-225 ± 14	-257 ± 11
50	-230 ± 13	-262 ± 9
Flat	-217 ± 14	-248 ± 7
Flat 30% anionic	-205 ± 11	-260 ± 6

The complex was then placed at vesicles of radius 50, 100, 250, and 500 Å starting from the final structure after MD in water and was simulated for a further 2 ns. Fig. 5 shows the final conformations on the different size vesicles. Binding is very tight on the smaller vesicles when E140 is protonated. Table 1 shows the transfer energy from water to the membrane at vesicles of different radius and the flat membrane. The difference in binding energy between protonated and unprotonated Glu140 at high curvatures is sufficient to "pay" the cost of protonation.

To characterize the shape of the complex in the different vesicles we report in Table 2 the spatial extent when the complex is aligned with the xy plane (Δx=Xmax-Xmin, and so on). The height of the complex is smaller when E140 is protonated and it is smallest for the 10-nm vesicle. At that curvature the complex resembles most the cryoEM structure. Asymmetry is larger when E140 is ionized.

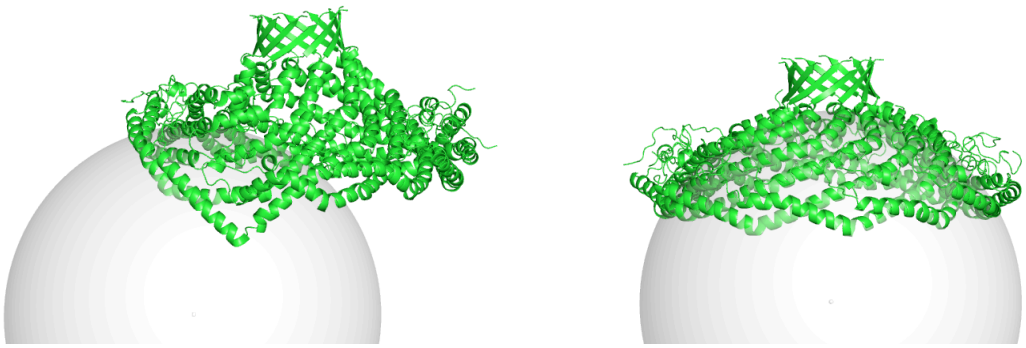

a) R= 5 nm

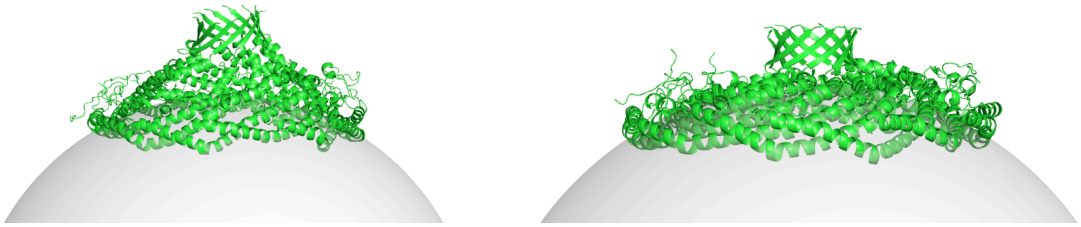

b) R= 10 nm

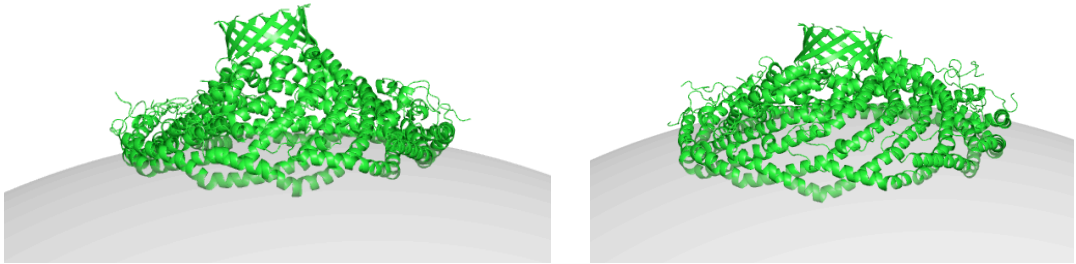

c) R= 25 nm

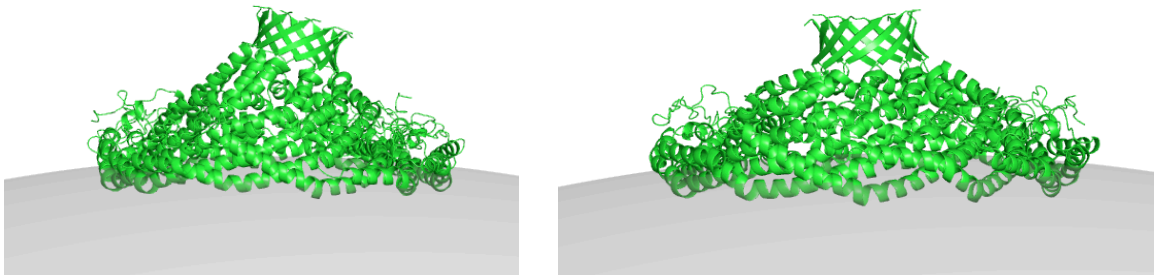

d) R= 50 nm

Fig. 5. Conformation of 8S on vesicles of different radius. E140 is ionized on the left and protonated on the right. a) R=5 nm, b) R=10 nm, c) R=25 nm, d) R=50 nm.

Table 2. Spatial extent of the complex on the different membranes in Å. The standard deviations are 1-4 Å. The values in the cryoEM structure are 137.4, 137.4, 40.1.

Radius (nm)	Δx, Δy, Δz ($E140^-$)	Δx, Δy, Δz (E140-H)
5	133.6, 127.2, 71.3	134.3, 130.2, 63.6
10	137.1, 128.0, 67.9	140.3, 135.1, 52.4
25	144.0, 128.9, 64.0	136.0, 130.7, 59.4
50	141.9, 130.1, 63.7	135.9, 130.7, 59.7
Flat	143.7, 128.5, 63.2	134.4, 131.1, 56.1
Water	138.8, 128.8, 61.9	134.5, 125.5, 60.4

DISCUSSION

The structures resulting from the simulations reported here depart significantly from the recent cryoEM structure (14) as well as earlier lower resolution work (23, 24) that show the caveolin 8S complex to be a flat disk. This would normally lead us to discount the simulation results as artifacts of the imperfections of the energy functions. However, because they make more mechanistic sense than the experimental structures, it is worth entertaining the possibility that some experimental factor biases the experimental structures toward flatter structures. The biggest difference between the in silico and in vitro systems is the presence of large amounts of detergent in the latter (dodecyl maltoside (14, 23) or octyl glucoside (24)). Structural work seems to be quite sensitive to the type of detergent used (25). Detergent covers 60% of the surface area of the complex, including much of the central cavity (14). It is not immediately clear how the detergent would flatten the disk, given that detergents are usually mobile and pliable and can adapt to a given shape. We plan to investigate this in the future by including detergent in the simulations.

A residue with a profound effect on binding to curved membranes was found to be E140. This residue is also E in cav3 and V in cav2. It can be hydrophobic or polar in other species (26). To our knowledge, there has not been any experimental investigation of this residue. We can only speculate on its role. Is it there to moderate binding affinity and thus allow caveolae to dissolve in response to mechanical stress? Does it impart pH sensitivity? In any case, it is an obvious target for mutation. It should be noted that cav1 is palmitoylated at three nearby positions (133,143,156). These palmitoyl groups, which are not included in the present simulations or in the cryoEM structure, would certainly increase the attachment to membranes. Nevertheless, palmitoylation is not necessary for localization in caveolae (27).

Electron microscopy has shown that caveolae have a polyhedral shape and that cav1 forms the inner part of the coat and cavin 1 the outer layer, with filaments running parallel to the edges of the polyhedra (28). Heterologous caveolae, i.e. structures formed in E. Coli after heterologous expression of cav1, also have polyhedral shape (5, 29). A model for the structure of cavin oligomers has also been proposed (24). The flatness of 8S led to the proposal that it binds the flat faces of the polyhedra (14, 24). But then, what deforms the membrane in the absence of cavins? If 8S can sense and generate membrane curvature itself, it may actually occupy not the flat faces but the vertices of the polyhedra observed in EM. The connections between the vertices could perhaps be provided by the missing, disordered N-terminal domains which could adopt defined structure under the right conditions.

The common size of caveolae is 50-80 nm in diameter (30), and heterologous caveolae in E. Coli induced by cav1 alone are 45-50 nm (5). Here we find stronger binding to smaller vesicles of diameter 10 and 20 nm. Several comments can be made in regard to this discrepancy. First, the transfer energy that we compute is not the full free energy of the protein (it does not include any intramolecular distortion energy of the complex). Second, the diameter of a vesicle is determined by a balance between binding energy and membrane deformation energy, which tends to keep the membrane flat. This energy is also not included in our calculation. Finally, if the 8S truly occupy the vertices of the polyhedra, the local curvature there will likely be higher than the overall curvature of the caveolae.

The caveolin story seems to offer one more example in the membrane remodeling field where the monomer by itself is irrelevant. It is the properties of the oligomer that determine function. This has also been recently suggested for the septins, although their structure is not yet known (31). In previous work from this lab, the same was suggested for the IBAR domains (20), but is not yet experimentally confirmed. Scaffolding by an oligomer is thus a strongly plausible mechanism for membrane curvature generation.

Acknowledgments

We thank the National Science Foundation (MCB-1855942) for funding and Dr. Amedee Des Georges for useful discussions.

Declaration of Interest

The authors declare no competing interests

Author contributions

TL conceived the project and wrote the article. SYVR conducted the simulations, analyzed the data, and prepared the figures with a small contribution from TL.

References

1. Parton, R.G. 2018. Caveolae: Structure, Function, and Relationship to Disease. Annu. Rev. Cell Dev. Biol. 34: 111–136.
2. Cheng, J.P.X., and B.J. Nichols. 2016. Caveolae: One Function or Many? Trends Cell Biol. 26: 177–189.
3. Williams, T.M., and M.P. Lisanti. 2004. The caveolin proteins. Genome Biol. 5: 1–8.
4. Kovtun, O., V.A. Tillu, N. Ariotti, R.G. Parton, and B.M. Collins. 2015. Cavin family proteins and the assembly of caveolae. J. Cell Sci. 128: 1269–1278.
5. Walser, P.J., N. Ariotti, M. Howes, C. Ferguson, R. Webb, D. Schwudke, N. Leneva, K.J. Cho, L. Cooper, J. Rae, M. Floetenmeyer, V.M.J. Oorschot, U. Skoglund, K. Simons, J.F. Hancock, and R.G. Parton. 2012. Constitutive formation of caveolae in a bacterium. Cell. 150: 752–763.
6. Lolo, F.N., N. Walani, E. Seemann, D. Zalvidea, D.M. Pavón, G. Cojoc, M. Zamai, C. Viaris de Lesegno, F. Martínez de Benito, M. Sánchez-Álvarez, J.J. Uriarte, A. Echarri, D. Jiménez-Carretero, J.C. Escolano, S.A. Sánchez, V.R. Caiolfa, D. Navajas, X. Trepat, J. Guck, C. Lamaze, P. Roca-Cusachs, M.M. Kessels, B. Qualmann, M. Arroyo, and M.A. del Pozo. 2023. Caveolin-1 dolines form a distinct and rapid caveolae-independent mechanoadaptation system. Nat.

Cell Biol. 25: 120–133.
7. Dupree, P., R.G. Parton, G. Raposo, T. V. Kurzchalia, and K. Simons. 1993. Caveolae and sorting in the trans-Golgi network of epithelial cells. EMBO J. 12: 1597–1605.
8. Parton, R.G., M. Hanzal-Bayer, and J.F. Hancock. 2006. Biogenesis of caveolae: A structural model for caveolin-induced domain formation. J. Cell Sci. 119: 787–796.
9. Lee, J., and K.J. Glover. 2012. The transmembrane domain of caveolin-1 exhibits a helix-break-helix structure. Biochim. Biophys. Acta - Biomembr. 1818: 1158–1164.
10. Rui, H., K.T. Root, J. Lee, K.J. Glover, and W. Im. 2014. Probing the U-shaped conformation of caveolin-1 in a bilayer. Biophys. J. 106: 1371–1380.
11. Park, S., K.J. Glover, and W. Im. 2019. U-shaped caveolin-1 conformations are tightly regulated by hydrogen bonds with lipids. J. Comput. Chem. 40: 1570–1577.
12. Liu, H., L. Yang, Q. Zhang, L. Mao, H. Jiang, and H. Yang. 2016. Probing the structure and dynamics of caveolin-1 in a caveolae-mimicking asymmetric lipid bilayer model. Eur. Biophys. J. 45: 511–521.
13. Prakash, S., A. Krishna, and D. Sengupta. 2021. Caveolin induced membrane curvature and lipid clustering: Two sides of the same coin? Faraday Discuss. 232: 218–235.
14. Porta, J.C., B. Han, A. Gulsevin, J.M. Chung, Y. Peskova, S. Connolly, H.S. McHaourab, J. Meiler, E. Karakas, A.K. Kenworthy, and M.D. Ohi. 2022. Molecular architecture of the human caveolin-1 complex. Sci. Adv. 8.
15. Lazaridis, T., and M. Karplus. 1999. Effective energy function for proteins in solution. Proteins Struct. Funct. Bioinforma. 35: 133–152.
16. Best, R.B., X. Zhu, J. Shim, P.E.M. Lopes, J. Mittal, M. Feig, and A.D. MacKerell. 2012. Optimization of the additive CHARMM all-atom protein force field targeting improved sampling of the backbone φ, ψ and side-chain χ1 and χ2 Dihedral Angles. J. Chem. Theory Comput. 8: 3257–3273.
17. Lazaridis, T. 2003. Effective energy function for proteins in lipid membranes. Proteins Struct. Funct. Bioinforma. 52: 176–192.
18. Nepal, B., J. Leveritt, and T. Lazaridis. 2018. Membrane Curvature Sensing by Amphipathic Helices: Insights from Implicit Membrane Modeling. Biophys. J. 114: 2128–2141.
19. Nepal, B., A. Sepehri, and T. Lazaridis. 2020. Mechanisms of negative membrane curvature sensing and generation by ESCRT III subunit Snf7. Protein Sci. 29: 1473–1485.
20. Nepal, B., A. Sepehri, and T. Lazaridis. 2021. Mechanism of negative membrane curvature generation by I-BAR domains. Structure. 29: in press.
21. Lazaridis, T. 2005. Structural determinants of transmembrane beta-barrels. J. Chem. Theory Comput. 1: 716–722.
22. Brooks, B.R., C.L. Brooks 3rd, A.D. Mackerell Jr., L. Nilsson, R.J. Petrella, B. Roux, Y. Won, G. Archontis, C. Bartels, S. Boresch, A. Caflisch, L. Caves, Q. Cui, A.R. Dinner, M. Feig, S. Fischer, J. Gao, M. Hodoscek, W. Im, K. Kuczera, T. Lazaridis, J. Ma, V. Ovchinnikov, E. Paci, R.W. Pastor, C.B. Post, J.Z. Pu, M. Schaefer, B. Tidor, R.M. Venable, H.L. Woodcock, X. Wu, W. Yang, D.M. York, and M. Karplus. 2009. CHARMM: the biomolecular simulation program. J. Comput. Chem. 30: 1545–1614.

23. Whiteley, G., R.F. Collins, and A. Kitmitto. 2012. Characterization of the molecular architecture of human caveolin-3 and interaction with the skeletal muscle ryanodine receptor. J. Biol. Chem. 287: 40302–40316.
24. Stoeber, M., P. Schellenberger, C.A. Siebert, C. Leyrat, K. Grünewald, and A. Helenius. 2016. Model for the architecture of caveolae based on a flexible, net-like assembly of Cavin1 and Caveolin discs. Proc. Natl. Acad. Sci. U. S. A. 113: E8069–E8078.
25. Han, B., J.C. Porta, J.L. Hanks, Y. Peskova, E. Binshtein, K. Dryden, D.P. Claxton, H.S. McHaourab, E. Karakas, M.D. Ohi, and A.K. Kenworthy. 2020. Structure and assembly of CAV1 8S complexes revealed by single particle electron microscopy. Sci. Adv. 6: 1–12.
26. Han, B., L.F.L. Wilson, A. Gulsevin, J. Meiler, E. Karakas, and A.K. Kenworthy. 2022. Design principles of caveolins across metazoa and beyond. bioRxiv. : 2022.11.15.516482.
27. Dietzen, D.J., W.R. Hastings, and D.M. Lublin. 1995. Caveolin is palmitoylated on multiple cysteine residues. Palmitoylation is not necessary for localization of caveolin to caveolae. J. Biol. Chem. 270: 6838–6842.
28. Ludwig, A., B.J. Nichols, and S. Sandin. 2016. Architecture of the caveolar coat complex. J. Cell Sci. 129: 3077–3083.
29. Ariotti, N., J. Rae, N. Leneva, C. Ferguson, D. Loo, S. Okano, M.M. Hill, P. Walser, B.M. Collins, and R.G. Parton. 2015. Molecular characterization of caveolin-induced membrane curvature. J. Biol. Chem. 290: 24875–24890.
30. Richter, T., M. Floetenmeyer, C. Ferguson, J. Galea, J. Goh, M.R. Lindsay, G.P. Morgan, B.J. Marsh, and R.G. Parton. 2008. High-resolution 3D quantitative analysis of caveolar ultrastructure and caveola-cytoskeleton interactions. Traffic. 9: 893–909.
31. Shi, W., K.S. Cannon, B.N. Curtis, C. Edelmaier, A.S. Gladfelter, and E. Nazockdast. 2023. Curvature sensing as an emergent property of multiscale assembly of septins. Proc. Natl. Acad. Sci. U. S. A. 120: 1–12.

Figure legends

Fig. 1. Structure of 8S before simulation (left), after a 5-ns MD simulation in implicit solvent (middle), and after a 3-ns MD simulation in explicit solvent (right). Side views above and top views below.

Fig. 2. 5-ns implicit solvent simulation in solution. a) Backbone RMS deviation with respect to the initial and the final structure, b) Spatial extent of the complex (the values for the cryoEM structure are 137.4, 137.4, 40.1 Å)

Fig. 3. Backbone RMSD (a) and spatial extent (b) and as a function of time in a 3-ns all-atom simulation in water.

Fig. 4. Conformation of 8S on a flat implicit membrane.

Fig. 5. Conformation of 8S on vesicles of different radius. E140 is ionized on the left and protonated on the right. a) R=5 nm, b) R=10 nm, c) R=25 nm, d) R=50 nm